ESC-TR-2001-074

Project Report
FPR-14

Analysis of SAR Image Formation Equations for Stationary and Moving Targets

A.F. Yegulalp

20 June 2002

Lincoln Laboratory
MASSACHUSETTS INSTITUTE OF TECHNOLOGY
LEXINGTON, MASSACHUSETTS

Prepared for the Defense Advanced Research Projects Agency
under Air Force Contract F19628-00-C-0002.

This report is based on studies performed at Lincoln Laboratory, a center for research operated by Massachusetts Institute of Technology. This work was sponsored by the Defense Advanced Research Projects Agency, IXO, under Air Force Contract F19628-00-C-0002.

The ESC Public Affairs Office has reviewed this report, and it is releasable to the National Technical Information Service, where it will be available to the general public, including foreign nationals.

This technical report has been reviewed and is approved for publication.

FOR THE COMMANDER

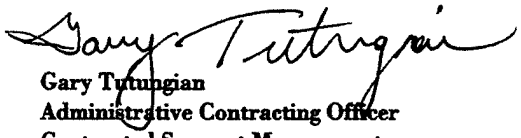

Gary Tutungian
Administrative Contracting Officer
Contracted Support Management

Massachusetts Institute of Technology
Lincoln Laboratory

Analysis of SAR Image Formation Equations for Stationary and Moving Targets

A.F. Yegulalp
Group 45

Project Report FPR-14

20 June 2002

Lexington Massachusetts

ABSTRACT

This report presents a detailed mathematical analysis of backprojection and "ω-k" (range migration) image formation equations for synthetic aperture radar (SAR). The image processor transfer function is computed for both stationary and moving targets, including antenna and target pattern effects. Assuming straight-line platform motion, it is demonstrated that both image formation algorithms provide exact focusing of stationary targets. Moving targets are displaced to false locations and blurred into elliptic or hyperbolic curves. Algorithms are suggested which will exactly refocus moving targets in SAR images based on only one unknown motion parameter. All results are derived without narrow-band, narrow-angle, or narrow-swath assumptions.

Similar derivations for moving target signatures and focusing algorithms have been presented in [1]. Reference [1] also demonstrates the application of moving target focusing to experimental data.

ACKNOWLEDGMENTS

The author would like to thank Dr. Jen K. Jao for useful discussions on moving target focusing and experiences with experimental data. Thanks are also due to Keith W. Forsythe, who provided initial calculations which motivated analysis of the $\omega - \mathrm{k}$ algorithm.

TABLE OF CONTENTS

LIST OF ILLUSTRATIONS

1. INTRODUCTION

1.1 SAR GEOMETRY

Figure 1 shows the basic geometry for a synthetic aperture radar (SAR) data collection. The radar platform is assumed to follow a straight-line trajectory, with its antenna beam illuminating terrain to one side of the aircraft. Points on the terrain surface may be labeled according to the along track (cross-range) coordinate x and the cross-track (slant-range) coordinate y. The so-called "slant-plane" coordinates (x,y) are natural for image formation, and will be used throughout this report. Note that y is by definition positive. Converting from the slant-plane coordinates to fixed "real-world" coordinates (e.g., latitude-longitude-elevation) is straightforward, but does require precise knowledge of the terrain contour and the flight track geometry.

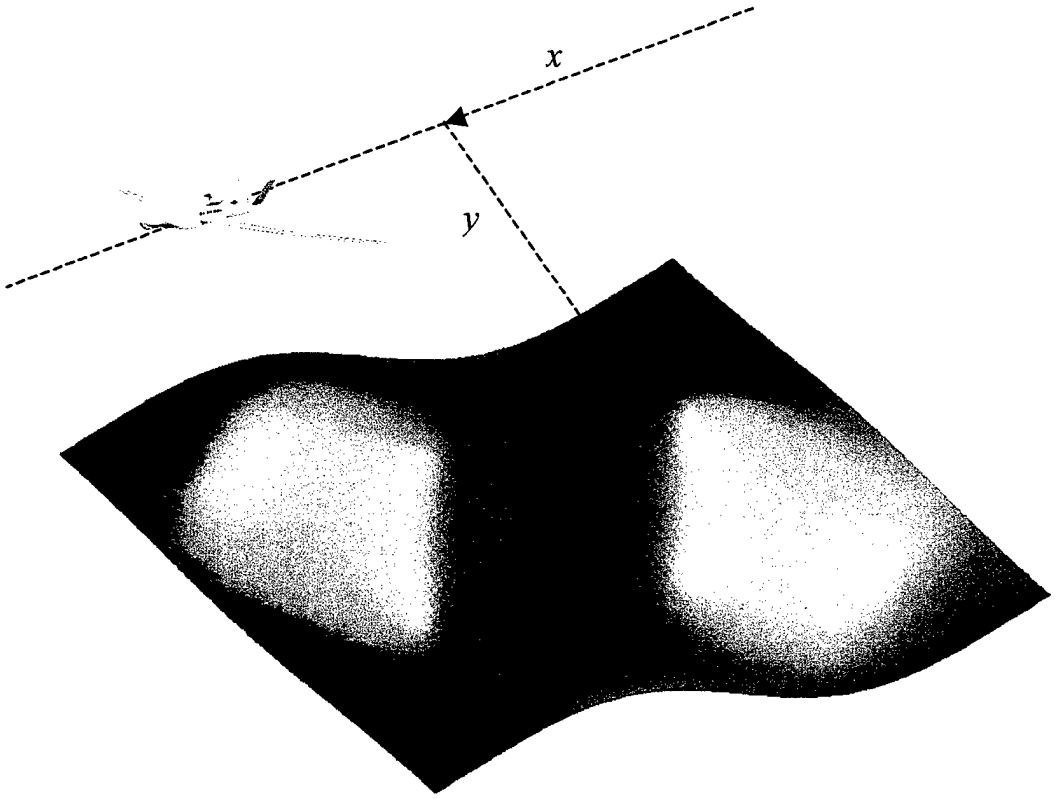

Figure 1. SAR flight geometry.

In practice, the aircraft will deviate somewhat from a straight-line path. Both image formation algorithms studied in this report can be adapted to compensate for off-track motion, but only the backprojection algorithm can provide exact image focusing for arbitrary aircraft motion and ground topography. To reduce the scope and complexity of the analysis in this report, all calculations will be performed for strictly straight-line motion.

Figure 2 shows the radar platform moving past a stationary target on the ground. A fixed antenna beam is assumed, illuminating a region of angular width θ_{ant} on the ground. Most of this document will assume that the beam is uniform within the angle θ_{ant} and zero outside. Section 4 will show how arbitrary antenna patterns may be accommodated using a simple modification of the uniform beam results.

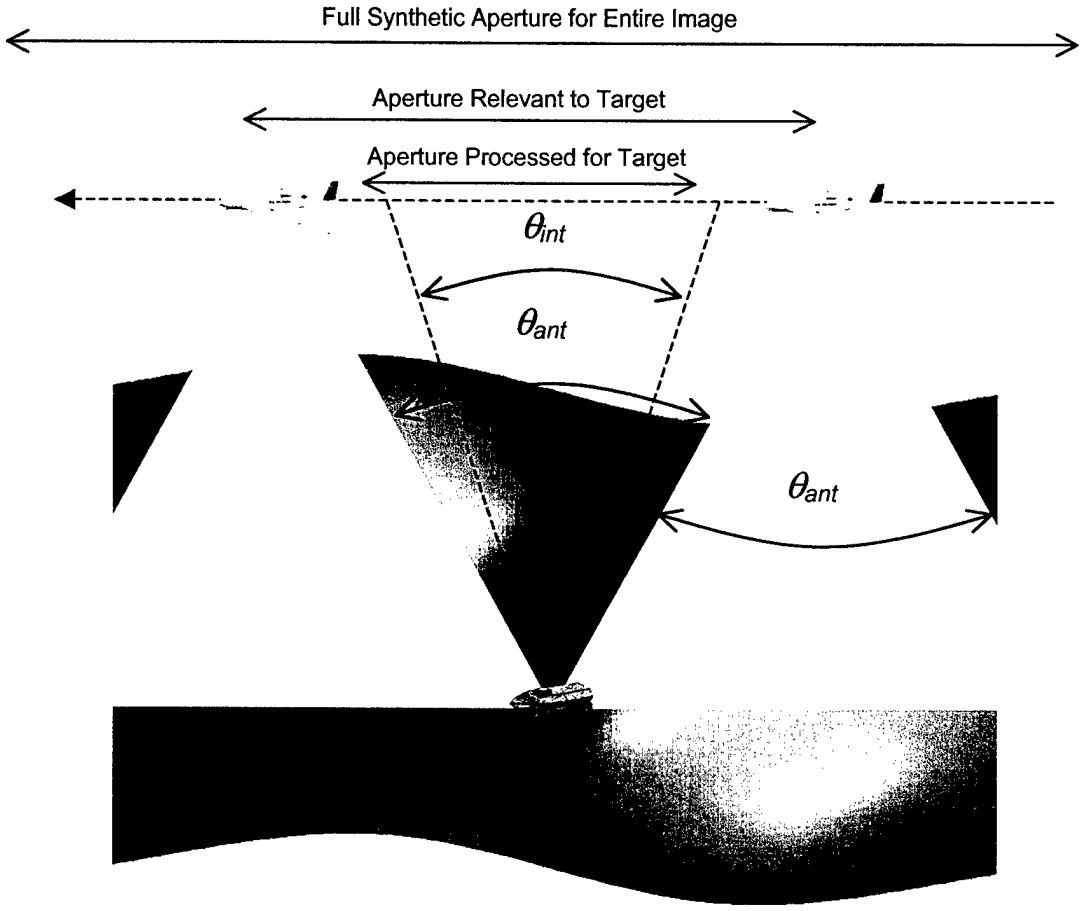

Figure 2. Beam and aperture geometry.

From the point of view of the target, the platform sweeps out an aperture of angular width θ_{ant} during the time it illuminates the target. The SAR processor may use any part of the full aperture in forming an image.

In stripmap-mode SAR, the processed aperture corresponds to a user-selected integration angle $\theta_{int} \leq \theta_{ant}$. Cross-range resolution in the image improves as θ_{int} is increased. Using a constant integration angle throughout the image produces an image with spatially invariant resolution and sidelobe structure. Note that the processed aperture is referenced with respect to the point being imaged, so different points in the image will be formed using different portions of the full aperture. Moreover, the length of the processed aperture will be proportional to range in order to maintain a constant integration angle.

Spotlight-mode SAR uses all available aperture data to form the image. Spotlight-mode radars also may employ a steerable beam to maintain illumination on a fixed patch on the ground over a longer aperture. For clarity of exposition, this document will focus on stripmap-mode SAR, but most results (aside from antenna pattern effects) extend to spotlight-mode in a straightforward manner.

1.2 SAR DATA MODEL

1.2.1 "Hopping" Model

As the radar platform moves along the synthetic aperture, it transmits a series of pulses and records the resulting backscatter. To simplify analysis, a "hopping" model will be used in which the platform hops forward from one pulse to the next, but remains stationary during the transmission and reception of each pulse. The approximation causes negligible errors as long as

$$TB < 0.1 \frac{c}{|dR/dt|}, \tag{1}$$

where T is the pulse length, B is the transmit bandwidth, c is the speed of light, and dR/dt is the range rate of change for ground points in the radar beam [2,3]. Typically the constraint is easily satisfied for airborne platforms, but may be violated for orbital platforms.

The hopping model may also be applied to moving targets. The target is assumed to move between pulses, but remain stationary during each pulse. Equation (1) determines the validity of the hopping model for moving targets, provided that the range rate dR/dt includes the combined effect of platform and target motion.

1.2.2 Range Compressed Pulse Data

No particular assumptions will be made regarding the radar waveform. Instead, it will simply be assumed that the return pulses are range compressed so that an ideal point scatterer[1] with unit cross section at range R will yield the signal

$$S(t,R)=\frac{B}{R^2}e^{2\pi i f_c(t-2R/c)}\,\mathrm{sinc}\big(B(t-2R/c)\big), \tag{2}$$

where B is the radar bandwidth, f_c is the center frequency, and $\mathrm{sinc}(u)\equiv\frac{\sin(\pi u)}{\pi u}$. Expressed in the frequency domain, Equation (2) is an integral over a flat spectrum:

$$S(t,R)=\frac{1}{R^2}\int_{f_{\min}}^{f_{\max}} e^{2\pi i f(t-2R/c)}\,df\,. \tag{3}$$

The minimum and maximum frequencies f_{min} and f_{max} are related to the radar bandwidth and center frequency by $f_{\min}=f_c-B/2$ and $f_{\max}=f_c+B/2$.

The range-compressed pulse data will be denoted by $D(\xi,t)$, where ξ is the radar position along the aperture and t is elapsed time after pulse transmission. If there is just a single stationary point scatterer at (x_0,y_0) with unit scattering amplitude, the target range is

$$R_0(\xi)=\sqrt{(x_0-\xi)^2+y_0^2}\,, \tag{4a}$$

and the range-compressed data is

$$D_0(\xi,t)=S\big(t,R_0(\xi)\big)\,. \tag{4b}$$

If the terrain is described by a complex scattering amplitude density $G(x,y)$, the range compressed data will be

$$D(\xi,t)=\iint G(x,y)S\left(t,\sqrt{(x-\xi)^2+y^2}\right)\,dxdy\,. \tag{5}$$

The case of a single point scatterer is equivalent to $G(x,y)=\delta(x-x_0)\delta(y-y_0)$.

[1] By definition, an ideal point scatterer has constant scattering amplitude as a function of frequency and direction.

Equations (2) through (5) implicitly assume uniform gain in frequency and direction for both the radar antenna and the terrain scattering. The more realistic case of nonuniform gain will be addressed in Section 4.

1.2.3 Moving Target Model

Consider a point scatterer target moving at constant velocity (with respect to slant plane coordinates). Working within the assumptions of the hopping model of Section 1.2.1, the corresponding range-compressed data can be written as

$$D_m(\xi,t) = S\left(t, R_m(\xi)\right), \tag{6a}$$

where the target range is

$$R_m(\xi) = \sqrt{(x_m - \xi)^2 + y_m^2} \tag{6b}$$

and the target coordinates are

$$\begin{aligned} x_m &= x_0 + u_x(\xi - x_0) \\ y_m &= y_0 + u_y(\xi - x_0) \end{aligned} \tag{7}$$

The target motion is parameterized using the broadside position (x_0,y_0) and the normalized velocity components (u_x,u_y). The broadside position is simply the position of the target at the moment when it is directly broadside to the aircraft (i.e., when $\xi=x_m$). The normalized velocity components are the target velocity components (v_x,v_y) divided by the platform speed $v_{platform}$:

$$\begin{aligned} u_x &= \frac{v_x}{v_{platform}} \\ u_y &= \frac{v_y}{v_{platform}} \end{aligned} \tag{8}$$

Straightforward algebraic manipulation shows that

$$R_m(\xi) = \sqrt{\gamma^2(\xi - x_s)^2 + y_s^2}\,, \tag{9}$$

where

$$\gamma = \sqrt{(1-u_x)^2 + u_y^2}\,, \qquad x_s = x_0 - \frac{u_y}{\gamma^2} y_0, \qquad \text{and} \qquad y_s = \frac{|1-u_x|}{\gamma} y_0. \tag{10}$$

The new quantities defined in Equation (10) all play important roles in the upcoming results. It will be shown that the motion parameter γ completely determines point target defocusing: at a given range, targets with the same γ have the same blurring. (Note that γ may be understood in physical terms as the target speed measured in the rest frame of the aircraft and normalized by the aircraft speed). It will also be shown that the quantities x_s and y_s are the shifted (apparent) coordinates of the target in the image.

For later notational convenience, the parameter ε is defined:

$$\varepsilon = 1 - \frac{1}{\gamma^2} = \frac{-2u_x + u^2}{1 - 2u_x + u^2}. \tag{11}$$

Stationary targets correspond to $\gamma = 1$ and $\varepsilon = 0$. Both γ and ε will be used freely in writing results, but it should be remembered that they are not independent quantities.

1.3 SAR AS A LINEAR SYSTEM

The process of SAR data collection can be thought of as a linear mapping $\mathbf{L}_{\mathbf{DC}}$ that transforms the terrain scattering amplitude into the range compressed data:

$$\mathbf{L}_{\mathbf{DC}}\{G(x,y)\} = D(\xi,t).$$

The transformation is linear in the sense that a linear combination of scattering amplitudes will map into a linear combination of range-compressed data:

$$\mathbf{L}_{\mathbf{DC}}\{\alpha G_1(x,y) + \beta G_2(x,y)\} = \alpha \mathbf{L}_{\mathbf{DC}}\{G_1(x,y)\} + \beta \mathbf{L}_{\mathbf{DC}}\{G_2(x,y)\}.$$

SAR image formation can also be thought of as a linear transformation $\mathbf{L}_{\mathbf{IF}}$. It maps the range-compressed data into the image data, attempting to recover the original terrain scattering amplitude:

$$I(x,y) = \mathbf{L}_{\mathbf{IF}}\{D(\xi,t)\} = \mathbf{L}_{\mathbf{IF}}\left\{\mathbf{L}_{\mathbf{DC}}\{G(x,y)\}\right\} \approx G(x,y).$$

The recovery can only be approximate due to the limitations of finite radar bandwidth and aperture. In general, the image is a filtered version of *G(x,y)*. The properties of any given image formation algorithm can be completely characterized by computing the transfer function of the aggregate transformation $\mathbf{L}_{\mathbf{IF}}\mathbf{L}_{\mathbf{DC}}$. By linearity, it suffices to compute the image function resulting from a point scatterer with unit scattering amplitude.

The analysis presented in Sections 2 and 3 will focus on computing the image spatial spectrum $\tilde{I}(k_x,k_y) = \frac{1}{(2\pi)^2}\iint dx\,dy\, I(x,y)e^{-ik_x x - ik_y y}$. Starting from the stationary point scatterer data

in Equation (4), it will be shown that both the backprojection and ω-k image formation equations produce

$$\tilde{I}(k_x,k_y)=\begin{cases} e^{-ix_0k_x-iy_0k_y} & \text{for } (k_x,k_y)\in\Omega \\ 0 & \text{for } (k_x,k_y)\notin\Omega \end{cases}. \tag{12}$$

The band-support region Ω is illustrated in Figure 3, and defined as follows:

$$\Omega=\left\{ (k_x,k_y) \;\middle|\; f_{min}<\tfrac{c}{4\pi}k<f_{max},\quad k_y>0 \text{ and } \frac{|k_x|}{k}<\sin\frac{\theta_{int}}{2} \right\},$$

$$\text{where } k\equiv\sqrt{k_x^2+k_y^2}\,. \tag{13}$$

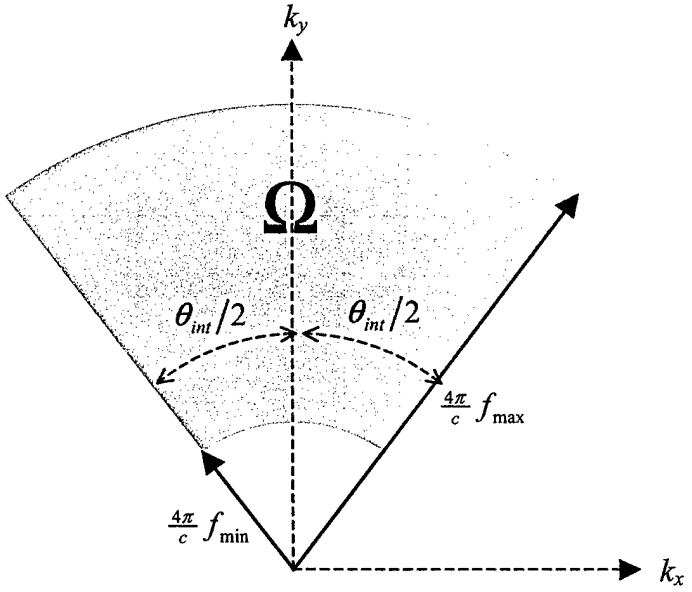

Figure 3. Band support region Ω for SAR image.

Equation (12) shows that the backprojection and ω-k image formation equations have ideal bandpass transfer functions. In other words, the image is a bandpassed version of the original scattering amplitude *G(x,y)*, with no extra phases or amplitude factors introduced. The size and

shape of the band-support region Ω reflects the transmitted waveform bandwidth, carrier frequency, and processed integration angle.

1.4 MOVING TARGETS IN SAR IMAGES

One of the basic assumptions in standard SAR image formation is that targets and clutter do not move while being illuminated by the radar beam. If a target does move, it will generally appear blurred and displaced to a false location in the image. The analysis in Sections 2 and 3 will consider a moving point target and derive the resulting image in both the spectral and spatial domains. In the spectral domain, the moving target image data looks like the stationary target result of Equation (12) multiplied by a nonlinear phase function and a nonconstant amplitude function. In the spatial domain, the moving target is blurred into an elliptic or hyperbolic arc.

The derived moving target signature may be used as the basis of an algorithm that reprocesses a standard SAR image to focus moving targets (and consequently blurs stationary targets). Despite the fact that the target velocity has two independent components, it will be shown that there is only one effective motion parameter that controls moving target focusing. In other words, an algorithm that seeks to focus moving targets of unknown velocity need only search over a *one*-dimensional space of possible focusing parameters. A second parameter is required only for precise compensation of motion-related distortions in the target and antenna patterns.

A closely related discussion of moving target focusing is presented in [1].

2. BACKPROJECTION IMAGE FORMATION

2.1 BACKPROJECTION EQUATION

Given range-compressed data $D(\xi,t)$, define the backprojection preprocessed data by

$$F_{BP}(\xi,t)=\frac{1}{2\pi i}\left(\frac{4\pi}{c}\right)^2\frac{\partial D(\xi,t)}{\partial t}. \tag{14}$$

The backprojection image is given by the equation

$$I(x,y)=y\int_{x-y\tan\frac{\theta_{int}}{2}}^{x+y\tan\frac{\theta_{int}}{2}}F_{BP}\left(\xi,\tfrac{2}{c}\sqrt{(x-\xi)^2+y^2}\right)d\xi \tag{15}$$

The basic backprojection algorithm has been discussed in a number of places in the SAR literature [3,4]. The exact details of the backprojection equation vary somewhat among different authors; the preceding definitions are chosen to yield an ideal bandpass transfer function.

In practice, Equations (14) and (15) are applied to digitally sampled data. The integral in Equation (15) is approximated using a sum over discrete aperture positions. Computing the integrand in Equation (15) requires a suitable interpolation in t for $F_{BP}(\xi,t)$.

The derivative in Equation (14) must also be adapted to discrete data. The easiest approach is to combine the derivative with the range compression process. Frequently compression is performed by convolving a matched filter $M(t)$ with raw pulse data $D_{raw}(\xi,t)$. The derivative is given by

$$\frac{\partial D(\xi,t)}{\partial t}=\frac{\partial}{\partial t}\int D_{raw}(\xi,t')M(t-t')dt'=\int D_{raw}(\xi,t')\frac{\partial M(t-t')}{\partial t}dt'.$$

In other words, the derivative can be applied just once to the matched filter $M(t)$ prior to any processing. The range compressed data will then automatically be differentiated, with no extra computation required. The derivative of a discretely sample matched filter can be performed easily in the frequency domain by multiplying by a factor of frequency.

In recent years, a number of accelerated backprojection algorithms have been developed [5–7]. The accelerated algorithms do not change the basic structure of Equations (14) and (15). Instead, they break the required numerical calculations into stages of increasing resolution, organized to reduced the total number of operations. The analysis in this section should apply equally well to any of the accelerated backprojection algorithms.

2.2 STATIONARY PHASE ANALYSIS (STATIONARY TARGET)[2]

Assume that the radar illuminates a stationary point scatterer target, as described in Section 1.2.2. The range compressed data is given by Equation (4b). Plugging the range compressed data into Equation (14) yields the backprojection preprocessed data:

$$F_{BP}(\xi,t)=\left(\frac{4\pi}{cR_0(\xi)}\right)^2 \int_{f_{min}}^{f_{max}} f\, e^{2\pi i f\left(t-\frac{2}{c}R_0(\xi)\right)}\, df\,. \tag{16}$$

Plugging Equation (16) into the backprojection Equation (15) and computing the spatial spectrum yields the four-dimensional integral

$$\tilde{I}(k_x,k_y)=\frac{4}{c^2}\int_0^{\infty} dy \int_{-\infty}^{\infty} dx \int_{x-y\tan\frac{\theta_{int}}{2}}^{x+y\tan\frac{\theta_{int}}{2}} d\xi \int_{f_{min}}^{f_{max}} df\, \frac{yf}{R_0(\xi)^2} e^{-ixk_x-iyk_y+\frac{4\pi i f}{c}\left(\sqrt{(x-\xi)^2+y^2}-R_0(\xi)\right)}\,. \tag{17}$$

The remainder of this section will be devoted to evaluating Equation (17) using the method of stationary phase[3].

The first step is to make the following change of variables:

$$\omega=\frac{4\pi}{c}f,\ \chi=x-\xi,\ \text{and}\ \ \zeta=\xi-x_0\,. \tag{18}$$

The spatial spectrum becomes

$$\tilde{I}(k_x,k_y)=\frac{1}{4\pi^2}e^{-ix_0k_x}\int_0^{\infty} dy \int_{-y\tan\frac{\theta_{int}}{2}}^{y\tan\frac{\theta_{int}}{2}} d\chi \int_{-\infty}^{\infty} d\zeta \int_{\frac{4\pi}{c}f_{min}}^{\frac{4\pi}{c}f_{max}} d\omega\, \frac{y\omega}{\zeta^2+y_0^2} e^{i\Phi(\chi,y,\zeta,\omega)}, \tag{19}$$

where the phase function Φ is defined as

$$\Phi(\chi,y,\zeta,\omega)=-\chi k_x-\zeta k_x-yk_y+\omega\sqrt{\chi^2+y^2}-\omega\sqrt{\zeta^2+y_0^2}\,. \tag{20}$$

The first derivatives of Φ are

---

[2] The stationary target case is, of course, subsumed within the moving target case treated in Section 2.4. The reader may regard the stationary target calculation as a "warm-up" for the more general discussion to come.

[3] See Appendix for a brief review of the multidimensional stationary phase approximation.

$$\frac{\partial\Phi}{\partial\chi} = -k_x + \frac{\chi\omega}{\sqrt{\chi^2+y^2}} \qquad \frac{\partial\Phi}{\partial\zeta} = -k_x - \frac{\zeta\omega}{\sqrt{\zeta^2+y_0^2}}$$

$$\frac{\partial\Phi}{\partial y} = -k_y + \frac{y\omega}{\sqrt{\chi^2+y^2}} \qquad \frac{\partial\Phi}{\partial\omega} = \sqrt{\chi^2+y^2} - \sqrt{\zeta^2+y_0^2}\,. \tag{21}$$

Solving the equation $\nabla\Phi = (\frac{\partial\Phi}{\partial\chi}, \frac{\partial\Phi}{\partial y}, \frac{\partial\Phi}{\partial\zeta}, \frac{\partial\Phi}{\partial\omega}) = 0$ shows that there is a single stationary point $(\chi, y, \zeta, \omega) = (\hat{\chi}, \hat{y}, \hat{\zeta}, \hat{\omega})$, where

$$\hat{\chi} = y_0 \frac{k_x}{|k_y|}, \qquad \hat{y} = y_0\,\mathrm{sgn}(k_y), \qquad \hat{\zeta} = -y_0 \frac{k_x}{|k_y|}, \text{ and } \qquad \hat{\omega} = k \equiv \sqrt{k_x^2+k_y^2}\,. \tag{22}$$

(Note that $y_0 > 0$ since slant range is an intrinsically positive quantity). If the stationary point falls outside the integration limits of Equation (19), the integral is zero. A simple analysis shows that the stationary point is inside the limits of integration if and only if $(k_x, k_y) \in \Omega$, where

$$\Omega = \left\{ (k_x, k_y) \;\middle|\; f_{\min} < \tfrac{c}{4\pi}k < f_{\max}, \quad k_y > 0 \text{ and } \frac{|k_x|}{k} < \sin\tfrac{\theta_{\text{int}}}{2} \right\}. \tag{23}$$

The band support region Ω is illustrated in Figure 3. The matrix of second derivatives of Φ is

$$\partial^2\Phi = \begin{pmatrix} \dfrac{y^2\omega}{(\chi^2+y^2)^{3/2}} & -\dfrac{\chi y\omega}{(\chi^2+y^2)^{3/2}} & 0 & \dfrac{\chi}{\sqrt{\chi^2+y^2}} \\ -\dfrac{\chi y\omega}{(\chi^2+y^2)^{3/2}} & \dfrac{\chi^2\omega}{(\chi^2+y^2)^{3/2}} & 0 & \dfrac{y}{\sqrt{\chi^2+y^2}} \\ 0 & 0 & -\dfrac{y_0^2\omega}{(\zeta^2+y_0^2)^{3/2}} & -\dfrac{\zeta}{\sqrt{\zeta^2+y_0^2}} \\ \dfrac{\chi}{\sqrt{\chi^2+y^2}} & \dfrac{y}{\sqrt{\chi^2+y^2}} & -\dfrac{\zeta}{\sqrt{\zeta^2+y_0^2}} & 0 \end{pmatrix}. \tag{24}$$

A tedious but straightforward computation gives the determinant:

$$\det \partial^2 \Phi = \frac{y_0^2 \omega^2}{\sqrt{\chi^2 + y^2}\left(\zeta^2 + y_0^2\right)^{3/2}}. \tag{25}$$

Plugging in the values from Equation (22) for the stationary point yields

$$\partial^2 \hat{\Phi} = \partial^2 \Phi(\hat{\chi}, \hat{y}, \hat{\zeta}, \hat{\omega}) = \begin{pmatrix} \frac{k_y^3}{y_0 k^2} & -\frac{k_x k_y^2}{y_o k^2} & 0 & \frac{k_x}{k} \\ -\frac{k_x k_y^2}{y_o k^2} & \frac{k_x^2 k_y}{y_0 k^2} & 0 & \frac{k_y}{k} \\ 0 & 0 & -\frac{k_y^3}{y_0 k^2} & \frac{k_x}{k} \\ \frac{k_x}{k} & \frac{k_y}{k} & \frac{k_x}{k} & 0 \end{pmatrix} \tag{26}$$

and

$$\det \partial^2 \hat{\Phi} = \frac{k_y^4}{y_0^2 k^2}. \tag{27}$$

The determinant is positive definite since $k_y \neq 0$ in the band support region Ω. Consequently, $\partial^2 \hat{\Phi}$ cannot have any zero eigenvalues. A numerical eigenanalysis with $k_x = k_y = y_0 = 1$ shows that there are two positive and two negative eigenvalues. Any continuous deformation of the parameters k_x, k_y, and y_0 will results in a continuous deformation of the eigenvalues. Since eigenvalues cannot cross zero, it follows there will always be two positive and two negative eigenvalues. Consequently,

$$\operatorname{sig} \partial^2 \hat{\Phi} = 2 - 2 = 0. \tag{28}$$

Combining the information from Equations (22), (27), and (28) with the stationary phase Equation (A.8) leads to the result

$$\tilde{I}(k_x, k_y) = \begin{cases} e^{-ix_0 k_x - iy_0 k_y} & \text{for } (k_x, k_y) \in \Omega \\ 0 & \text{for } (k_x, k_y) \notin \Omega \end{cases}. \tag{29}$$

Equation (29) shows that the backprojection image formation equation has an ideal bandpass transfer function. In other words, the image is a bandpassed version of the original scattering amplitude *G(x,y)*, with no extra phases or amplitude factors introduced. The size and shape of the band-support region Ω reflects the transmitted waveform bandwidth, carrier frequency, and processed integration angle.

2.3 IMPACT OF PREPROCESSING STEP

It is possible to form images without performing the preprocessing step in Equation (14). In other words, the image is computed directly from the range-compressed data:

$$I(x,y) = y \int_{x-y\tan\frac{\theta_{int}}{2}}^{x+y\tan\frac{\theta_{int}}{2}} D\left(\xi, \frac{2}{c}\sqrt{(x-\xi)^2+y^2}\right) d\xi . \tag{30}$$

Equation (30) may be analyzed exactly as in Section 2.2. The only change is that the integrand in Equation (17) loses a factor of f and some multiplicative constants. Since the phase function Φ is the same, the coordinates of the stationary point in Equation (22) and the matrix of second derivatives in Equation (24) remain unchanged. The final result is

$$\tilde{I}(k_x,k_y) = \begin{cases} \frac{c}{4\pi k} e^{-ik_x x_0 - ik_y y_0} & \text{for } (k_x,k_y) \in \Omega \\ 0 & \text{for } (k_x,k_y) \notin \Omega \end{cases} . \tag{31}$$

Comparing Equations (31) to (29) shows that skipping the preprocessing step introduces a non-uniform gain factor proportional to $1/k$. For ultra-wideband radar, the extra non-uniform gain factor can have a measurable impact on resolution and sidelobe structure in the image.

2.4 MOVING TARGET ANALYSIS

2.4.1 Stationary Phase Calculation of Image Spectrum

Consider a point scatterer target moving at constant velocity, as modeled in Section 1.2.3. The moving target data may be processed into an image using the standard backprojection Equations (14) and (15). The resulting image will be analyzed in this section using the same stationary phase analysis applied to the stationary target case in Section 2.2. Putting the range-compressed data from Equation (6a) into the preprocessing Equation (14) yields

$$F_{BP}(\xi,t)=\left(\frac{4\pi}{cR_m(\xi)}\right)^2 \int_{f_{\min}}^{f_{\max}} f\, e^{2\pi i f\left(t-\frac{2}{c}R_m(\xi)\right)}\, df\,. \tag{32}$$

Plugging the preprocessed data from Equation (32) into the backprojection Equation (15) and computing the spatial spectrum yields the four-dimensional integral

$$\tilde{I}(k_x,k_y)=\frac{4}{c^2}\int_0^{\infty}dy\int_{-\infty}^{\infty}dx\int_{x-y\tan\frac{\theta_{\text{int}}}{2}}^{x+y\tan\frac{\theta_{\text{int}}}{2}}d\xi\int_{f_{\min}}^{f_{\max}}df\,\frac{yf}{R_m(\xi)^2}e^{-ixk_x-iyk_y+\frac{4\pi if}{c}\left(\sqrt{(x-\xi)^2+y^2}-R_m(\xi)\right)}. \tag{33}$$

Note that Equation (33) is the same as the stationary target case in Equation (17), except for the substitution $R_0 \to R_m$. The remainder of this section will be devoted to evaluating Equation (33) using the method of stationary phase[4].

The first step is to make the following change of variables:

$$\omega=\frac{4\pi}{c}f,\ \chi=x-\xi,\ \text{and}\ \ \zeta=\gamma(\xi-x_s)\,. \tag{34}$$

The spatial spectrum becomes

$$\tilde{I}(k_x,k_y)=\frac{1}{4\pi^2\gamma}e^{-ix_sk_x}\int_0^{\infty}dy\int_{-y\tan\frac{\theta_{\text{int}}}{2}}^{y\tan\frac{\theta_{\text{int}}}{2}}d\chi\int_{-\infty}^{\infty}d\zeta\int_{\frac{4\pi}{c}f_{\min}}^{\frac{4\pi}{c}f_{\max}}d\omega\,\frac{y\omega}{\zeta^2+y_s^2}e^{i\Phi(\chi,y,\zeta,\omega)}, \tag{35}$$

where the phase function Φ is defined as

$$\Phi(\chi,y,\zeta,\omega)=-\chi k_x-\frac{\zeta k_x}{\gamma}-yk_y+\omega\sqrt{\chi^2+y^2}-\omega\sqrt{\zeta^2+y_s^2}\,. \tag{36}$$

The first derivatives of Φ are

$$\frac{\partial\Phi}{\partial\chi}=-k_x+\frac{\chi\omega}{\sqrt{\chi^2+y^2}} \qquad \frac{\partial\Phi}{\partial\zeta}=-\frac{k_x}{\gamma}-\frac{\zeta\omega}{\sqrt{\zeta^2+y_s^2}}$$

[4] See Appendix for a brief review of the multidimensional stationary phase approximation.

$$\frac{\partial \Phi}{\partial y} = -k_y + \frac{y\omega}{\sqrt{\chi^2 + y^2}} \qquad \frac{\partial \Phi}{\partial \omega} = \sqrt{\chi^2 + y^2} - \sqrt{\zeta^2 + y_s^2} \,. \tag{37}$$

Solving the equation $\nabla\Phi = (\frac{\partial\Phi}{\partial\chi}, \frac{\partial\Phi}{\partial y}, \frac{\partial\Phi}{\partial\zeta}, \frac{\partial\Phi}{\partial\omega}) = 0$ provides the stationary point coordinates

$$\hat{\chi} = y_s \frac{k_x}{\sqrt{k_y^2 + \varepsilon k_x^2}} \qquad \hat{\zeta} = -y_s \frac{k_x}{\gamma\sqrt{k_y^2 + \varepsilon k_x^2}}$$

$$\hat{y} = y_s \frac{k_y}{\sqrt{k_y^2 + \varepsilon k_x^2}} \qquad \hat{\omega} = k \equiv \sqrt{k_x^2 + k_y^2} \,, \tag{38}$$

where $\varepsilon \equiv 1 - \frac{1}{\gamma^2}$.

If the stationary point falls outside the integration limits of Equation (35), the integral is zero. A simple analysis shows that the stationary point is inside the limits of integration if and only if $(k_x, k_y) \in \Omega_\gamma$, where

$$\Omega_\gamma = \left\{ (k_x, k_y) \;\middle|\; f_{\min} < \tfrac{c}{4\pi} k < f_{\max}, \quad k_y > 0 \text{ and } \frac{|k_x|}{k} < \min\left(\sin\tfrac{\theta_{\text{int}}}{2}, \gamma\right) \right\}. \tag{39}$$

If $\gamma \geq \sin(\theta_{\text{int}}/2)$, the band-support region Ω_γ is the same as in the stationary target case illustrated in Figure 3. If $\gamma < \sin(\theta_{\text{int}}/2)$, the angular width of the band support region is reduced as shown in Figure 4.

The matrix of second derivatives of Φ is

$$\partial^2\Phi = \begin{pmatrix} \dfrac{y^2\omega}{\left(x^2+y^2\right)^{3/2}} & -\dfrac{xy\omega}{\left(x^2+y^2\right)^{3/2}} & 0 & \dfrac{x}{\sqrt{x^2+y^2}} \\ -\dfrac{xy\omega}{\left(x^2+y^2\right)^{3/2}} & \dfrac{x^2\omega}{\left(x^2+y^2\right)^{3/2}} & 0 & \dfrac{y}{\sqrt{x^2+y^2}} \\ 0 & 0 & -\dfrac{y_s^2\omega}{\left(\zeta^2+y_s^2\right)^{3/2}} & -\dfrac{\zeta}{\sqrt{\zeta^2+y_s^2}} \\ \dfrac{x}{\sqrt{x^2+y^2}} & \dfrac{y}{\sqrt{x^2+y^2}} & -\dfrac{\zeta}{\sqrt{\zeta^2+y_s^2}} & 0 \end{pmatrix}. \tag{40}$$

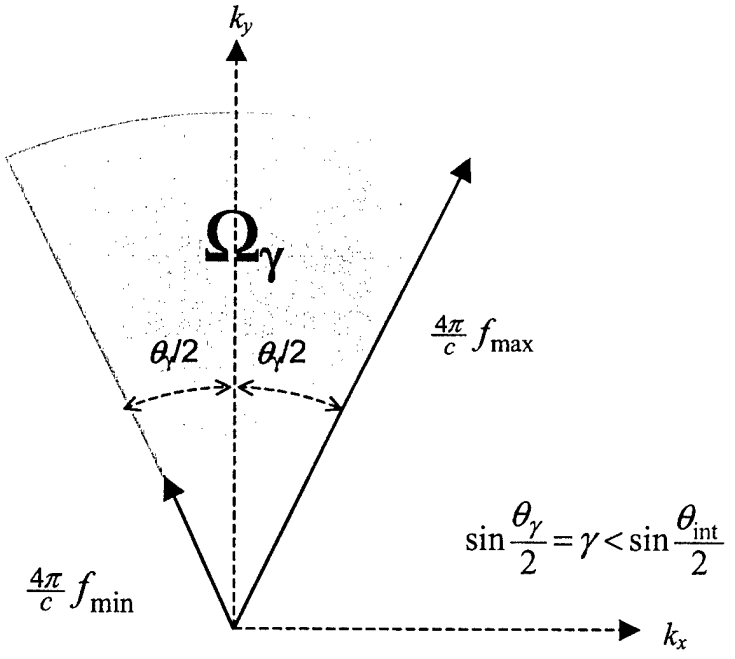

Figure 4. Band support region Ω_γ for moving target SAR image when $\gamma < \sin(\theta_{\text{int}}/2)$.

A tedious but straightforward computation gives the determinant:

$$\det \partial^2 \Phi = \frac{y_s^2 \omega^2}{\sqrt{\chi^2 + y^2}\left(\zeta^2 + y_s^2\right)^{3/2}}. \tag{41}$$

Plugging in the values from Equation (38) for the stationary point yields

$$\partial^2 \hat{\Phi} = \partial^2 \Phi(\hat{\chi}, \hat{y}, \hat{\zeta}, \hat{\omega}) = \begin{pmatrix} \frac{k_y^2 \sqrt{k_y^2 + \varepsilon k_x^2}}{y_s k^2} & -\frac{k_x k_y \sqrt{k_y^2 + \varepsilon k_x^2}}{y_s k^2} & 0 & \frac{k_x}{k} \\ -\frac{k_x k_y \sqrt{k_y^2 + \varepsilon k_x^2}}{y_s k^2} & \frac{k_x^2 \sqrt{k_y^2 + \varepsilon k_x^2}}{y_s k^2} & 0 & \frac{k_y}{k} \\ 0 & 0 & -\frac{\left(k_y^2 + \varepsilon k_x^2\right)^{3/2}}{y_s k^2} & \frac{k_x}{k\gamma} \\ \frac{k_x}{k} & \frac{k_y}{k} & \frac{k_x}{k\gamma} & 0 \end{pmatrix} \tag{42}$$

and

$$\det \partial^2 \hat{\Phi} = \frac{(k_y^2 + \varepsilon k_x^2)^2}{y_s^2 k^2}. \tag{43}$$

It may be easily shown that the determinant is positive definite in the band support region Ω_γ. Consequently, $\partial^2 \hat{\Phi}$ cannot have any zero eigenvalues. A numerical eigenanalysis with $k_x = k_y = y_s = 1$ and $\varepsilon = 0$ shows that there are two positive and two negative eigenvalues. Any continuous deformation of the parameters k_x, k_y, y_s, and ε will results in a continuous deformation of the eigenvalues. Since eigenvalues cannot cross zero, it follows there will always be two positive and two negative eigenvalues. Consequently,

$$\operatorname{sig} \partial^2 \hat{\Phi} = 2 - 2 = 0. \tag{44}$$

Combining the information from Equations (38), (43), and (44) with the stationary phase Equation (A.8) leads to the result

$$\tilde{I}(k_x,k_y)=\begin{cases}\dfrac{k_y}{\gamma\sqrt{k_y^2+\varepsilon k_x^2}}e^{-ix_sk_x-iy_s\sqrt{k_y^2+\varepsilon k_x^2}} & \text{for } (k_x,k_y)\in\Omega_\gamma \\ 0 & \text{for } (k_x,k_y)\notin\Omega_\gamma\end{cases}. \tag{45}$$

The spectrum depends on the target motion purely through the single motion parameter $\gamma=\sqrt{(1-u_x)^2+u_y^2}$. (Recall that the parameter ε is a function of γ, as defined in Equation (11)).

2.4.2 Moving Target Signature in Spatial Domain

The moving target signature in the spatial domain is given by the inverse Fourier transform of the spectrum in Equation (45):

$$I(x,y)=\iint dk_x\,dk_y\;\;\tilde{I}(k_x,k_y)e^{ixk_x+iyk_y}=\iint_{\Omega_\gamma} dk_x\,dk_y\,\frac{k_y}{\gamma\sqrt{k_y^2+\varepsilon k_x^2}}e^{i\Psi(k_x,k_y)}\;. \tag{46}$$

The phases have been collected into the function Ψ:

$$\Psi(k_x,k_y)=(x-x_s)k_x+yk_y-y_s\sqrt{k_y^2+\varepsilon k_x^2}\;. \tag{47}$$

The derivatives of the phase function are

$$\frac{\partial\Psi}{\partial k_x}=x-x_s-y_s\frac{\varepsilon k_x}{\sqrt{k_y^2+\varepsilon k_x^2}}\qquad\text{and}\qquad\frac{\partial\Psi}{\partial k_y}=y-y_s\frac{k_y}{\sqrt{k_y^2+\varepsilon k_x^2}}. \tag{48}$$

Solving the stationary phase equation $\nabla\Psi=(\frac{\partial\Psi}{\partial k_x},\frac{\partial\Psi}{\partial k_y})=0$ shows that there are no stationary points unless

$$\frac{1}{\varepsilon}(x-x_s)^2+y^2=y_s^2\qquad\text{and}\qquad y>0. \tag{49}$$

When Equation (49) holds, the stationary phase equation is solved by all points $(\hat{k}_x,\hat{k}_y)$, which satisfy

$$\frac{\hat{k}_x}{\hat{k}_y} = \frac{x - x_s}{\varepsilon y}. \tag{50}$$

In other words, the solution is a "stationary line" in the (k_x, k_y) plane rather than a single stationary point. Consequently, the stationary phase equations in the Appendix do not directly apply to Equation (46). The existence of a stationary line implies that $\det \partial^2 \Psi = 0$, so a formal evaluation using Equation (A.8) will produce a meaningless infinite answer. Nevertheless, the basic principle underlying the stationary phase method still applies to Equation (46): the integral should be "large" when stationary points exist and small otherwise. It follows that the blurred target will appear as a curve in the *(x,y)* plane satisfying Equation (49). For $\varepsilon > 0$ the curve will be elliptic, and for $\varepsilon < 0$ it will be hyperbolic. Equation (50) determines the length of the curve since the stationary points $(\hat{k}_x, \hat{k}_y)$ are required to lie in the band support region Ω_γ.

The curve of the blurred target signature may be written in parametric form as follows:

For $\varepsilon > 0$ (i.e., $\gamma > 1$):

$$x = x_s + \sqrt{\varepsilon}\, y_s \sin\varphi,$$

$$y = y_s \cos\varphi,$$

$$\text{where } |\tan\varphi| < \sqrt{\varepsilon}\, \min\left(\sin\tfrac{\theta_{\text{int}}}{2}, \gamma\right). \tag{51}$$

For $\varepsilon < 0$ (i.e., $\gamma < 1$):

$$x = x_s + \sqrt{|\varepsilon|}\, y_s \sinh\varphi,$$

$$y = y_s \cosh\varphi,$$

$$\text{where } |\tanh\varphi| < \sqrt{|\varepsilon|}\, \min\left(\sin\tfrac{\theta_{\text{int}}}{2}, \gamma\right). \tag{52}$$

The curves in Equations (51) and (52) are illustrated in Figure 5. Note that curves with $\varepsilon > 0$ always bend toward the flight track, while curves with $\varepsilon < 0$ curve away. The point (x_s, y_s) is the center point of the blurred target curve; it is related to the true target coordinates via Equation (10).

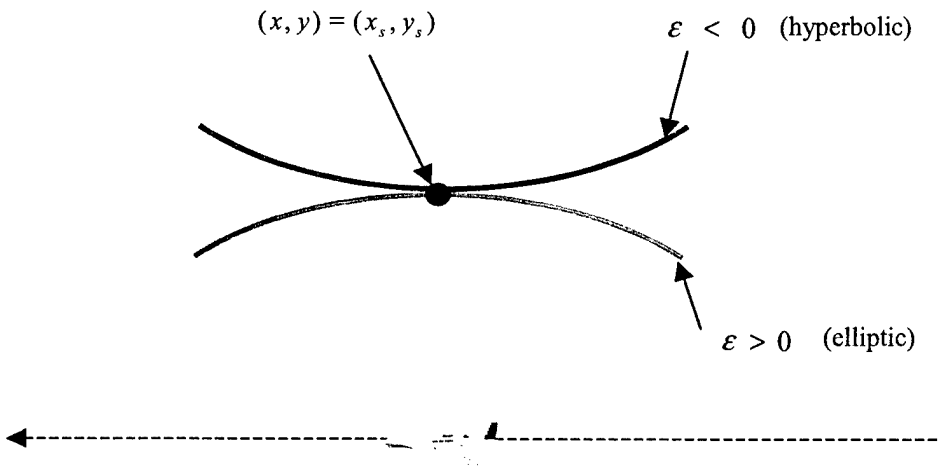

Figure 5. Moving target signature in spatial domain.

2.4.3 Expansion for Small Target Velocities

When $u_x << 1$ and $u_y << 1$, the following leading-order expansions become relevant:

$$\varepsilon \approx -2u_x, \qquad x_s \approx x_0 - u_y y_0, \qquad \text{and} \qquad y_s = y_0 - \frac{1}{2}u_y^2 y_0. \tag{53}$$

At leading order, defocusing (governed by ε) depends only on the along-track velocity component. Target displacement depends only on the cross-track velocity component, and there is no cross-track displacement at first order.

2.4.4 Refocusing Moving Target Images Via Spatially Variant Filtering

As demonstrated in the previous sections, a moving target will appear as an elliptic or hyperbolic streak in a standard SAR image. It is possible to "refocus" the SAR image so that all moving targets with $\varepsilon = \varepsilon_F$ at a given range $y = y_F$ appear well focused. Refocusing is accomplished by applying a filter with the following transfer function:

$$\tilde{U}(k_x, k_y; \varepsilon_F, y_F) = \frac{1}{\sqrt{1-\varepsilon_F}} \frac{\sqrt{k_y^2 + \varepsilon_F k_x^2}}{k_y} e^{iy_F\left(\sqrt{k_y^2+\varepsilon_F k_x^2} - k_y\right)}. \tag{54}$$

Applying the filter in Equation (54) to the moving target spectrum in Equation (45) produces the point target spectrum

$$\tilde{I}_F(k_x,k_y;\varepsilon_F,y_F)=\tilde{U}(k_x,k_y;\varepsilon_F,y_F)\,\tilde{I}(k_{x,},k_y)=e^{-ix_sk_x-iy_sk_y}, \tag{55}$$

provided that $\varepsilon=\varepsilon_F$ and $y_s=y_F$. If the filter parameters ε_F and y_F differ from the target parameters ε and y_s, focus quality will degrade.

The focusing filter may be applied by computing the two-dimensional FFT of the image data, multiplying by the transfer function Equation (54), and computing the inverse FFT. To provide exact focus at different ranges in the image, the entire process must be repeated with different values of y_F.

2.4.5 Refocusing Moving Targets Via Frequency-Domain Resampling

The method described in the previous section will correctly focus moving targets, but may require many filtering operations to cope with the range-dependence of the filter. This section will describe an alternative refocusing method that provides exact focus for all ranges simultaneously. The basic idea is to resample the frequency domain image data as follows:

$$\tilde{I}_F\left(k_x,k_y;\varepsilon_F\right)=\frac{1}{\sqrt{1-\varepsilon_F}}\frac{k_y}{\sqrt{k_y^2-\varepsilon_F k_x^2}}\tilde{I}\left(k_x,\sqrt{k_y^2-\varepsilon_F k_x^2}\right). \tag{56}$$

The coordinate transformation in Equation (56) is analogous to the Stolt transformation performed in the ω-k image formation algorithm [8]. Applying Equation (56) to the moving target spectrum in Equation (45) yields

$$\tilde{I}_F\left(k_x,k_y;\varepsilon_F\right)=\sqrt{\frac{1-\varepsilon}{1-\varepsilon_F}}\frac{k_y}{\sqrt{k_y^2+(\varepsilon-\varepsilon_F)k_x^2}}e^{-ix_sk_x-iy_s\sqrt{k_y^2+(\varepsilon-\varepsilon_F)k_x^2}}. \tag{57}$$

When $\varepsilon_F=\varepsilon$, the target is perfectly focused:

$$\tilde{I}_F\left(k_x,k_y;\varepsilon\right)=e^{-ix_sk_x-iy_sk_y}. \tag{58}$$

There is one important subtlety in Equation (56) that must be addressed for practical applications. The image spectrum $\tilde{I}$ in Equation (56) is the Fourier transform of the entire (infinite) image plane. In practice one works with $\tilde{I}^{data}$, the transform of a finite-sized array of image data centered on some point (x_c,y_c). The two are related as follows:

$$\tilde{I}^{data}(k_x,k_y)=\tilde{I}(k_x,k_y)e^{ix_ck_x+iy_ck_y}. \tag{59}$$

The same relation also applies to the refocused image. Combining Equations (56) and (59) leads to the result

$$\tilde{I}_F^{data}\left(k_x,k_y;\varepsilon_F\right)=\frac{1}{\sqrt{1-\varepsilon_F}}\frac{k_y}{\sqrt{k_y^2-\varepsilon_F k_x^2}}\tilde{I}^{data}\left(k_x,\sqrt{k_y^2-\varepsilon_F k_x^2}\right)\ e^{iy_c\left(k_y-\sqrt{k_y^2-\varepsilon_F k_x^2}\right)}. \quad (60)$$

Comparing Equations (60) to (56) shows that the extra phase factor $e^{iy_c\left(k_y-\sqrt{k_y^2-\varepsilon_F k_x^2}\right)}$ is required for focusing $\tilde{I}^{data}$. The refocusing process in Equation (60) becomes especially easy to understand when rewritten as a two step process $\tilde{I}^{data}\rightarrow\tilde{I}_1^{data}\rightarrow\tilde{I}_F^{data}$, where

$$\tilde{I}_1^{data}\left(k_x,k_y;\varepsilon_F\right)=\tilde{U}\left(k_x,k_y;\varepsilon_F,y_c\right)\tilde{I}^{data}\left(k_x,k_y\right) \quad (61)$$

$$\tilde{I}_F^{data}\left(k_x,k_y;\varepsilon_F\right)=\tilde{I}_1^{data}\left(k_x,\sqrt{k_y^2-\varepsilon_F k_x^2}\right). \quad (62)$$

The first step in Equation (61) applies the focusing filter $\tilde{U}$ specified in Equation (54); it provides exact focus for targets at range $y=y_c$. The second step in Equation (62) is a non-linear resampling in the k_y direction, which extends exact focus to *all* range values.

3. ω-K IMAGE FORMATION

This section will demonstrate, within the stationary phase approximation, that the ω-k image formation equation produces stationary and moving target signatures precisely identical to those produced by backprojection. A direct calculation for the stationary target case will be omitted, since it is just a special case of the moving target result.

3.1 IMAGE FORMATION EQUATION

The basic input to image formation is the range compressed data $D(\xi,t)$. The ω-k equation computes the image spatial spectrum directly:

$$\tilde{I}(k_x,k_y)=\begin{cases}\dfrac{k_y e^{\frac{i\pi}{4}}}{\sqrt{2\pi k}}\displaystyle\int_{-\infty}^{\infty}d\xi\int_{-\infty}^{\infty}dt\ \left(\tfrac{ct}{2}\right)^{3/2}D(\xi,t)\ e^{-ik_x\xi-\frac{i}{2}ckt} & \text{for } (k_x,k_y)\in\Omega,\\ 0 & \text{otherwise.}\end{cases} \tag{63}$$

The band support region Ω is defined according to Equation (13). As in previous sections, $k\equiv\sqrt{k_x^2+k_y^2}$. The image is computed by an inverse Fourier transform of $\tilde{I}$. More detailed discussion of the ω-k algorithm (also known as range migration) and its history may be found in [8]. In the published literature, there are some variations in the multiplicative factors included in Equation (63). The particular factors used above are chosen to yield an ideal bandpass transfer function.

3.2 STATIONARY PHASE ANALYSIS (MOVING TARGET)

Consider a point scatterer target moving at constant velocity, as modeled in Section 1.2.3. The range compressed data $D_m(\xi,t)$ is strongly peaked at $t=2R_m(\xi)/c$, which enables the following approximation:

$$\left(\tfrac{ct}{2}\right)^{3/2}D_m(\xi,t)\approx R_m(\xi)^{3/2}D_m(\xi,t). \tag{64}$$

A more rigorous approach to the approximation in Equation (64) is to regard it as the first term in a Taylor expansion of $t^{3/2}$ around the point $t=2R_m(\xi)/c$. A rather laborious calculation, not

reproduced here, shows that the correction to the image from the next term in the Taylor expansion is smaller by a factor of order $1/kR \sim \lambda/R$.

Inserting the moving target data into Equation (63) and applying the above approximation yields

$$\tilde{I}(k_x,k_y)=\frac{k_y e^{\frac{i\pi}{4}}}{\sqrt{2\pi k}}\int_{-\infty}^{\infty} d\xi \;\; R_m(\xi)^{3/2} e^{-ik_x\xi}\int_{-\infty}^{\infty} dt \;\; D_m(\xi,t) \;\; e^{-\frac{i}{2}ckt}. \tag{65}$$

To simplify the notation, it is assumed that $(k_x,k_y)\in\Omega$. The integral over t simply produces the Fourier transform of the range compressed data:

$$\int_{-\infty}^{\infty} dt \;\; D_m(\xi,t) \;\; e^{-\frac{i}{2}ckt} = \frac{1}{R_m(\xi)^2} e^{-ikR_m(\xi)} \tag{66}$$

Making the change of variable $\zeta=\gamma(\xi-x_s)$, Equation (65) becomes

$$\tilde{I}(k_x,k_y)=\frac{k_y e^{\frac{i\pi}{4}}}{\gamma\sqrt{2\pi k}}\int_{-\infty}^{\infty} d\xi \;\; \frac{1}{\sqrt{\zeta^2+y_s^2}} e^{i\Phi(\zeta)}, \tag{67}$$

where the phase function Φ is defined as

$$\Phi(\zeta)=-\frac{\zeta}{\gamma}k_x - k\sqrt{\zeta^2+y_s^2}. \tag{68}$$

The derivatives of the phase function are

$$\frac{\partial\Phi}{\partial\zeta}=-\frac{k_x}{\gamma}-\frac{k\zeta}{\sqrt{\zeta^2+y_s^2}} \quad \text{and} \quad \frac{\partial^2\Phi}{\partial\zeta^2}=-\frac{k}{\sqrt{\zeta^2+y_s^2}}+\frac{k\zeta^2}{\left(\zeta^2+y_s^2\right)^{3/2}}. \tag{69}$$

The stationary phase condition $\frac{\partial\Phi}{\partial\zeta}=0$ is satisfied at the point $\zeta=\hat{\zeta}$, where

$$\hat{\zeta}=-\frac{k_x y_s}{\gamma\sqrt{k_y^2+\varepsilon k_x^2}}. \tag{70}$$

The stationary point exists if and only if the condition $\frac{|k_x|}{k} < \gamma$ is satisfied. At the stationary point

$$\Phi(\hat{\zeta}) = -y_s\sqrt{k_y^2 + \varepsilon k_x^2} \qquad \text{and} \qquad \frac{\partial^2\Phi}{\partial\zeta^2}(\hat{\zeta}) = -\frac{\left(k_y^2 + \varepsilon k_x^2\right)^{3/2}}{k^2 y_s}. \tag{71}$$

Applying the stationary phase Equation (A.2) to the integral in Equation (67) yields

$$\tilde{I}(k_x, k_y) = \begin{cases} \dfrac{k_y}{\gamma\sqrt{k_y^2+\varepsilon k_x^2}} e^{-ix_s k_x - iy_s\sqrt{k_y^2+\varepsilon k_x^2}} & \text{for } (k_x, k_y) \in \Omega_\gamma \\ 0 & \text{for } (k_x, k_y) \notin \Omega_\gamma. \end{cases} \tag{72}$$

The modified band-support region Ω_γ is defined in Equation (39); it incorporates the condition $\frac{|k_x|}{k} < \gamma$ required for the existence of the stationary point. As promised, the $\omega - k$ image spectrum in Equation (72) is identical to the backprojection spectrum in Equation (45).

4. ANTENNA AND TARGET PATTERN EFFECTS

In previous sections, it was assumed that the SAR antenna has a transmission pattern uniform in frequency and direction. Similarly, it was assumed that the target and terrain scattering patterns are uniform. In this section, the uniformity assumptions will be relaxed, allowing arbitrary (but slowly varying) patterns instead.

Figure 6 shows the basic platform/target geometry. In slant plane coordinates, the platform position is $(\xi,0)$ and the target position is (x_m,y_m). The angle between the flight track and the line-of-sight to the target is κ. The patterns are expressed in terms of the complementary angle $\theta = \pi/2 - \kappa$ and the frequency f. Note that θ is also the angle with respect to broadside. The SAR antenna pattern will be denoted by the complex-valued function $A_{ant}(f,\theta)$, and the target scattering pattern by $A_{targ}(f,\theta)$. Both patterns also depend implicitly on the cross-track position of the target.

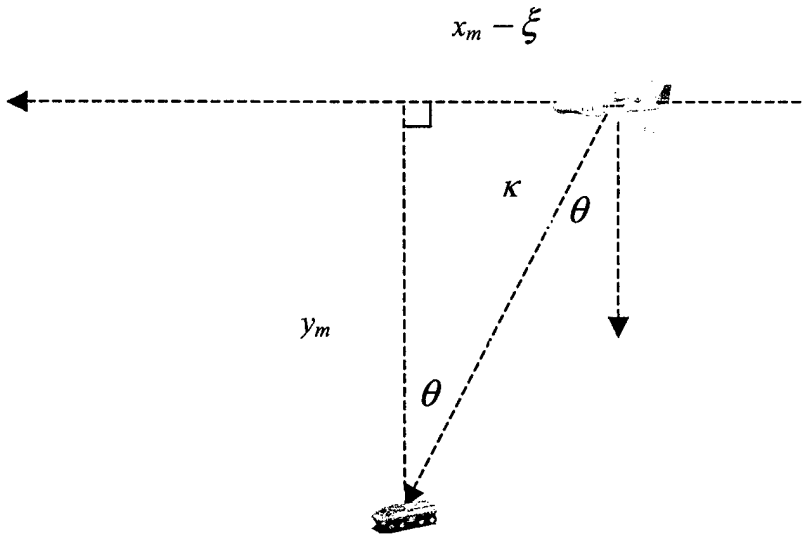

Figure 6. Platform/target geometry.

The angle θ is related to the platform position by the equation

$$\theta = \tan^{-1}\left(\frac{x_m - \xi}{y_m}\right). \tag{73}$$

The basic range compressed data of Equation (3) is easily modified to including the antenna and target pattern factors:

$$S(t,R)=\frac{1}{R^2}\int_{f_{\min}}^{f_{\max}} e^{2\pi i f(t-2R/c)}A_{ant}(f,\theta)A_{targ}(f,\theta)\,df\,. \tag{74}$$

4.1 STATIONARY TARGETS

For the stationary target case,

$$(x_m,y_m)=(x_0,y_0) \qquad \text{and} \qquad \theta=\tan^{-1}\left(\frac{x_0-\xi}{y_0}\right). \tag{75}$$

The backprojection stationary phase analysis in Section 2.2 may be repeated using the modified range compressed data in Equation (74). The antenna and target pattern factors propagate directly through the calculation to the final result. The stationary point coordinates are unchanged since the phase function Φ is not affected by the slowly varying pattern factors. The stationary point values for f and θ are

$$\hat{f}=\frac{c}{4\pi}k=\frac{c}{4\pi}\sqrt{k_x^2+k_y^2} \qquad \text{and} \qquad \hat{\theta}=\tan^{-1}\frac{k_x}{k_y}\,. \tag{76}$$

The backprojection image spectrum is

$$\tilde{I}(k_x,k_y)=\begin{cases} H_{ant}(k_x,k_y)H_{targ}(k_x,k_y)e^{-ix_0k_x-iy_0k_y} & \text{for } (k_x,k_y)\in\Omega \\ 0 & \text{for } (k_x,k_y)\notin\Omega, \end{cases} \tag{77}$$

where the antenna and target transfer functions are given by

$$\begin{aligned} H_{ant}(k_x,k_y)&=A_{ant}\left(\frac{c}{4\pi}k,\tan^{-1}\frac{k_x}{k_y}\right) \\ H_{targ}(k_x,k_y)&=A_{targ}\left(\frac{c}{4\pi}k,\tan^{-1}\frac{k_x}{k_y}\right). \end{aligned} \tag{78}$$

In short, the antenna and target patterns are manifested as filters that act on the slant-plane image data. Note that the relation between the H's and the A's is just a transformation between polar coordinates and Cartesian coordinates.

Despite the identical mathematical properties of the antenna and target patterns, there is an important distinction in terms of practical application. The target pattern will differ from target to target, providing useful information characterizing the targets. The antenna pattern is fixed, and it obviously provides no information about targets. Any nonlinear behavior in the phase of $H_{ant}(k_x,k_y)$ will cause blurring in the image.

To generate calibrated imagery, a post-image formation filter must be applied to compensate for the antenna pattern transfer function. The calibration filter is defined by inverting the transfer function of the antenna:

$$H_{cal}(k_x,k_y)=\frac{1}{H_{ant}(k_x,k_y)}. \tag{79}$$

In practice, the inversion will be approximate for several reasons. First, an FIR digital filter needs to have a finite number of taps. Second, the exact inversion in Equation (79) can become singular or nearly singular, which would result in undesirably large amplification of the noise floor. Finally, knowledge of the antenna pattern is almost certainly approximate, so it is pointless to attempt an exact inversion.

The calibrated image spectrum is

$$\tilde{I}_C(k_x,k_y)=\begin{cases} H_{targ}(k_x,k_y)e^{-ix_0k_x-iy_0k_y} & \text{for } (k_x,k_y)\in\Omega \\ 0 & \text{for } (k_x,k_y)\notin\Omega. \end{cases} \tag{80}$$

4.2 MOVING TARGETS

The moving target coordinates (x_m,y_m) are given in Equation (7). The backprojection stationary phase analysis in Section 2.4.1 may be repeated using the modified range compressed data in Equation (74). The antenna and target pattern factors propagate directly through the calculation to the final result. The stationary point coordinates are unchanged since the phase function Φ is not affected by the pattern factors. The stationary point values for f and θ are

$$\hat{f}=\frac{c}{4\pi}k=\frac{c}{4\pi}\sqrt{k_x^2+k_y^2} \qquad \text{and} \qquad \hat{\theta}=\psi+\tan^{-1}\left(\frac{k_x}{\gamma\sqrt{k_y^2+\varepsilon k_x^2}}\right). \tag{81}$$

The angle ψ describes the direction of the target velocity relative to the radar platform:

$$\psi = \tan^{-1}\frac{u_y}{1-u_x}. \tag{82}$$

The normalized target velocity components (u_x, u_y) can be expressed in terms of the motion parameters γ and ψ:

$$\begin{aligned} 1-u_x &= \gamma\cos\psi \\ u_y &= \gamma\sin\psi. \end{aligned} \tag{83}$$

The backprojection image spectrum (prior to antenna pattern calibration) is

$$\tilde{I}(k_x,k_y) = A_{targ}(\hat{f},\hat{\theta})A_{ant}(\hat{f},\hat{\theta})\tilde{I}_{nopat}(k_x,k_y), \tag{84}$$

where $\tilde{I}_{nopat}(k_x,k_y)$ is the moving target spectrum without pattern effects, as given in Equation (45). The pattern factors may be written in terms of the transfer functions defined in Equation (78):

$$A_{ant}(\hat{f},\hat{\theta}) = H_{ant}\left(\frac{k_x}{\gamma}\cos\psi + \sqrt{k_y^2+\varepsilon k_x^2}\sin\psi, \sqrt{k_y^2+\varepsilon k_x^2}\cos\psi - \frac{k_x}{\gamma}\sin\psi\right). \tag{85}$$

An analogous equation hold for A_{targ}.

Since the antenna pattern transfer function is modified by target motion, calibration becomes more complicated. In general, the calibration filter in Equation (79) will not compensate for the transfer function in Equation (85). The only exception is when the antenna pattern is independent of the direction θ. Target motion only affects the stationary point value of θ, not f, so the antenna pattern transfer function is the same as for stationary targets. The calibration filter of Equation (79) can be used to remove the antenna pattern effect, and then moving targets may be focused as described in Sections 2.4.4 and 2.4.5.

4.3 MOVING TARGET REFOCUSING AND CALIBRATION

The moving target refocusing algorithm of Section 2.4.5 may be applied as is to uncalibrated image data with nonuniform target and antenna patterns. In other words, the image data given by Equation (84) can be plugged directly into the refocusing formula of Equation (56). For a point target located at (x_0, y_0), the result is

$$\tilde{I}_F\left(k_x,k_y;\varepsilon\right)=H\left(\frac{k_x}{\gamma}\cos\psi+k_y\sin\psi,\ k_y\cos\psi-\frac{k_x}{\gamma}\sin\psi\right)e^{-ix_sk_x-iy_sk_y}, \qquad (86)$$

where

$$H(k_x,k_y)=H_{ant}(k_x,k_y)H_{targ}(k_x,k_y)$$

is the lumped transfer function of the antenna and target patterns. Note that Equation (86) assumes that the correct value of ε was used when applying the refocusing equation.

The antenna pattern in the refocused image can be removed by applying a calibration filter with the transfer function[5]

$$H_{cal}(k_x,k_y)=H\left(\frac{k_x}{\gamma}\cos\psi+k_y\sin\psi,\ k_y\cos\psi-\frac{k_x}{\gamma}\sin\psi\right)^{-1}. \qquad (87)$$

A key observation is that only one parameter (ε, or equivalently, γ) is required to focus moving targets, but the extra parameter ψ is required for antenna pattern calibration.

Even after applying antenna calibration with the correct value of ψ, Equation (86) shows that the target pattern is still distorted by a mix of rotation and stretching in the (k_x,k_y) plane. It is possible to obtain undistorted target patterns by using an alternative calibration procedure. Rather than applying the filter in Equation (87), the following transformation can be applied to the refocused image:

$$\tilde{I}_{F2}\left(k_x,k_y;\ \varepsilon,\psi\right)=\tilde{I}_F\left(\gamma k_x\cos\psi-\gamma k_y\sin\psi,\ k_x\sin\psi+k_y\cos\psi;\varepsilon\right). \qquad (88)$$

For the point target case, the result is

$$\tilde{I}_{F2}\left(k_x,k_y;\ \varepsilon,\psi\right)=H_{ant}(k_x,k_y)H_{targ}(k_x,k_y)e^{-ix_{FT}k_x-iy_{FT}k_y}. \qquad (89)$$

The coordinates (x_{FT},y_{FT}) are "fixed-time" coordinates of the moving target. In other words, they are the target coordinates at the time the platform reaches the position $\xi=0$ along the synthetic aperture. They are related to the broadside coordinates[6] (x_0,y_0) as follows:

[5] The inversion is to be understood with the same caveats that apply in the stationary target case.

[6] i.e., the position of the target when it is broadside to the SAR platform; see Equation (7).

$$x_{FT} = x_0(1-u_x) = x_0\gamma\cos\psi$$
$$y_{FT} = y_0 - u_y x_0 = y_0 - x_0\gamma\sin\psi. \tag{90}$$

The transformed image data in Equation (89) can then be calibrated using the ordinary stationary-target calibration filter in Equation (79). The target pattern is undistorted by virtue of the transformation in Equation (88). As a side benefit, the target image appears at the true fixed-time location (x_{FT}, y_{FT}), instead of the shifted position (x_s, y_s).

There are two important points practical points that are worth addressing here. The first point concerns the fact that true image data is typically centered on some point (x_c, y_c), while the above equations implicitly assume the image data is centered at zero. The matter was addressed in Section 2.4.5, and the same solution applies here. The second point is that the two-dimensional resampling step in Equation (88) would be easier and more efficient to implement in terms of two sequential *one*-dimensional resampling operations.

Taking the above-mentioned points into account, a multi-step procedure $\tilde{I}^{data} \to \tilde{I}_1^{data} \to \tilde{I}_2^{data} \to \tilde{I}_3^{data} \to \tilde{I}_4^{data} \to \tilde{I}_F^{data}$ is suggested for moving target focusing and antenna calibration. The steps are as follows:

$$\tilde{I}_1^{data}\left(k_x, k_y; \varepsilon_F\right) = \tilde{U}\left(k_x, k_y; \varepsilon_F, y_c\right)\tilde{I}^{data}\left(k_x, k_y\right) \tag{91}$$

$$\tilde{I}_2^{data}\left(k_x, k_y; \varepsilon_F\right) = \tilde{I}_1^{data}\left(k_x, \sqrt{k_y^2 - \varepsilon_F k_x^2}\right) \tag{92}$$

$$\tilde{I}_3^{data}\left(k_x, k_y;\ \varepsilon_F, \psi_F\right) = \tilde{I}_2^{data}\left(k_x, \frac{k_x}{\gamma}\tan\psi_F + k_y\sec\psi_F\ ;\ \varepsilon_F\right) \tag{93}$$

$$\tilde{I}_4^{data}\left(k_x, k_y;\ \varepsilon_F, \psi_F\right) = \tilde{I}_3^{data}\left(\gamma k_x\cos\psi_F - \gamma k_y\sin\psi_F,\ k_y;\ \varepsilon_F, \psi_F\right) \tag{94}$$

$$\tilde{I}_F^{data}\left(k_x, k_y;\ \varepsilon_F, \psi_F\right) = \frac{1}{H_{ant}(k_x, k_y)}\tilde{I}_4^{data}\left(k_x, k_y;\ \varepsilon_F, \psi_F\right). \tag{95}$$

The "data" superscript has the same meaning as in Section 2.4.5, indicating image data centered at (x_c, y_c). The first two steps in Equations (91) and (92) are precisely identical to the focusing algorithm given in Equations (61) and (62). The next two steps in Equations (93) and (94) perform one-dimensional resampling operations that undo the scaling and rotation effects in the antenna and target patterns. Note that the combined effect of Equations (93) and (94) is identical to that produced by Equation (88), but the latter requires a more complicated two-dimensional

resampling. Finally, Equation (95) calibrates the image by eliminating the antenna transfer function. Caveats discussed in the previous section regarding inversion of the antenna transfer function apply equally well here.

Applying Equations (91–95) to a point target with the correct values $\varepsilon_F = \varepsilon$ and $\psi_F = \psi$ produces the spectrum

$$\tilde{I}_F^{data}\left(k_x, k_y;\ \varepsilon, \psi\right) = H_{targ}(k_x, k_y) e^{-ix_{SFT}k_x - iy_{SFT}k_y}.$$

The target is focused at the "shifted fixed-time" coordinates (x_{SFT}, y_{SFT}) that are related to the "fixed-time" coordinates in Equation (90) as follows:

$$\begin{aligned} x_{SFT} &= x_{FT} + x_c(1-\gamma\cos\psi) - y_c\sin\psi \\ y_{SFT} &= y_{FT} + x_c\gamma\sin\psi + y_c(1-\cos\psi). \end{aligned} \tag{96}$$

A nice feature of the multistep focusing procedure above is that the operations occur in order of importance (most to least) as well as order of complexity (least to most). Applying the first step in Equation (91) requires just one focusing parameter, no resampling, and will mitigate most of the blurring due to target motion. The second step introduces no new parameters, requires only one-dimensional resampling, and extends focus to all ranges. The remaining steps require a second parameter and multiple resampling steps to achieve an undistorted target response with the antenna pattern removed. The number of steps actually implemented in a practical system can be chosen to suit the desired accuracy and available computing resources. Conceptually, each additional step makes a correction at a more subtle level than the previous one, with the full sequence providing an exactly focused and calibrated image.

APPENDIX
STATIONARY PHASE EQUATIONS

A.1 ONE DIMENSIONAL INTEGRALS

Consider an integral of the form

$$I = \int_V g(x) e^{i\mu\phi(x)} dx \,, \tag{A.1}$$

where $\phi(x)$ is strictly real-valued. As μ becomes large, the phase factor $e^{i\mu\phi(x)}$ will fluctuate rapidly. The rapid fluctuations tend to cancel out, except at stationary points where $\frac{\partial\phi}{\partial x} = 0$. Asymptotic analysis in the limit $\mu \to +\infty$ leads to the stationary phase equation

$$I \approx \sum_k \sqrt{\frac{2\pi}{|\mu\phi''(\hat{x}_k)|}} g(\hat{x}_k) e^{i\mu\phi(\hat{x}_k)} e^{\frac{i\pi}{4}\mathrm{sgn}(\phi''(\hat{x}_k))} \,. \tag{A.2}$$

The sum is over the set of stationary points $\hat{x}_k \in V$ where $\phi'(\hat{x}_k) = \frac{\partial\phi}{\partial x}\Big|_{x=\hat{x}_k} = 0$. If there are no stationary points in the integration region V, then $I \approx 0$ at leading order in the asymptotic expansion. The "sgn" function in Equation (A.2) simply returns the sign of its argument:

$$\mathrm{sgn}(x) = \begin{cases} +1 & \text{if } x > 0 \\ 0 & \text{if } x = 0 \\ -1 & \text{if } x < 0. \end{cases} \tag{A.3}$$

Equation (A.2) applies under "generic" conditions: $\phi''(\hat{x}_k) \neq 0$ and no stationary points on the boundaries of the integration region V. A careful derivation of (A.2) and discussion of conditions on the functions $\phi(x)$ and $g(x)$ may be found in a variety of references; an excellent exposition is provided in [9]. For the purposes of this document, the integrals evaluated are always of "generic" type and Equation (A.2) will be applied without further discussion of any subtleties.

The derivation of Equation (A.2) may be sketched as follows. At leading order, the only parts of the integral Equation (A.1) that matter are near the stationary points. In other words,

$$I \approx \sum_k \int_{\hat{x}_k - \varepsilon}^{\hat{x}_k + \varepsilon} g(x) e^{i\mu\phi(x)} dx = \sum_k \int_{-\varepsilon}^{\varepsilon} g(\hat{x}_k + s) e^{i\mu\phi(\hat{x}_k + s)} ds \tag{A.4}$$

for some suitable value of ε. Expanding ϕ to second order around the stationary point(s) and treating g as a constant yields

$$I \approx \sum_k g(\hat{x}_k) e^{i\mu\phi(\hat{x}_k)} \int_{-\varepsilon}^{\varepsilon} e^{\frac{i}{2}\mu\phi''(\hat{x}_k)(s-\hat{x}_k)^2} ds . \tag{A.5}$$

Since the integrand fluctuates rapidly for $|s| > \varepsilon$, the limits of integration may be extended to infinity without changing results at leading order. The resulting Gaussian integral may be computed exactly, producing the final result in Equation (A.2).

A.2 MULTIDIMENSIONAL INTEGRALS

The N-dimensional stationary phase integral is of the form

$$I = \int_V G(\mathbf{x}) e^{i\mu\Phi(\mathbf{x})} d^N\mathbf{x} . \tag{A.6}$$

The bold symbol $\mathbf{x}$ denotes an N-dimensional real vector, and $d^N\mathbf{x}$ denotes integration over the N components of $\mathbf{x}$. The stationary phase derivation proceeds exactly as in the one-dimensional case. The stationary points are $\hat{\mathbf{x}}_k \in V$ such that $\nabla\Phi(\hat{\mathbf{x}}_k) = 0$.

After expanding Φ to second order around the stationary point(s), the integral becomes

$$I \approx \sum_k G(\hat{\mathbf{x}}_k) e^{i\mu\Phi(\hat{\mathbf{x}}_k)} \int e^{\frac{i}{2}\mu\mathbf{s}^T\partial^2\Phi(\hat{\mathbf{x}}_k)\mathbf{s}} d^N\mathbf{s} . \tag{A.7}$$

The notation $\partial^2\Phi(\hat{\mathbf{x}}_k)$ represents the matrix of second derivatives of Φ at the k-th stationary point. Performing the Gaussian integral in Equation (A.7) leads to the N-dimensional stationary phase equation:

$$I \approx \sum_k \frac{(2\pi)^{N/2}}{\sqrt{\mu\left|\det\partial^2\Phi(\hat{\mathbf{x}}_k)\right|}} G(\hat{\mathbf{x}}_k) e^{i\mu\Phi(\hat{\mathbf{x}}_k)} e^{\frac{i\pi}{4}\mathrm{sig}\left(\partial^2\Phi(\hat{\mathbf{x}}_k)\right)} . \tag{A.8}$$

The matrix signature function in Equation (A.8) is a matrix generalization of the "sgn" function:

$$\mathrm{sig}(\mathbf{M}) = (\#\text{ of positive eigenvalues of } \mathbf{M}) - (\#\text{ of negative eigenvalues of } \mathbf{M}) .$$

REFERENCES

1. J. K Jao, "Theory of Synthetic Aperture Radar Imaging of a Moving Target," *IEEE Trans. Geosci. Remote Sens.*, vol. 39, No. 9, 1984–1992, September 2001.

2. A.W. Rihaczek, *Principles of High-Resolution Radar*, New York, McGraw-Hill, 1969.

3. J.L. Bauck and W.K. Jenkins, "Tomographic Processing of Spotlight-Mode Synthetic Aperture Radar Signals with Compensation for Wavefront Curvature," *ICASSP 88:1988 Int. Conf. Acoust., Speech, and Signal Process.*, Cat. No. 88CH2561-9, vol. 2, 1192–1195, IEEE, New York, 1988.

4. M.D. Desai and W.K. Jenkins, "Convolution Backprojection Image Reconstruction for Spotlight Mode Synthetic Aperture Radar," *IEEE Trans. on Image Proc.*, vol. 1, no. 4, 505–517, October 1992.

5. A.F. Yegulalp, "Fast Backprojection Algorithm for Synthetic Aperture Radar," *Proc. 1999 IEEE Int. Radar Conf.*, 60–65, April 20–22 1999, Waltham, Mass.

6. J. McCorkle and M. Rofheart, "An Order $N^2 logN$ Backprojector Algorithm for Focusing Wide-Angle Wide-Bandwidth Arbitrary-Motion Synthetic Aperture Radar," *SPIE - Int. Soc. Opt. Eng. Proceedings of Spie – the International Society for Optical Engineering*, vol. 2747, 25–36, 1996, Orlando, Fla.

7. S. Nilsson, L.-E. Andersson, "Application of Fast Backprojection Techniques for Some Inverse Problems of Synthetic Aperture Radar," *SPIE – Int. Soc. Opt. Eng. Proc.*, vol. 3370, 62–72, 1998, Orlando, Fla.

8. W.G. Carrara, R.S. Goodman, and R.M. Majewski, *Spotlight Synthetic Aperture Radar*, 333–335, Norwood, MA, Artech House, 1995.

9. C.M. Bender and S.A. Orszag, *Advanced Mathematical Methods for Scientists and Engineers*, 276–280, New York, McGraw-Hill, 1978.

REPORT DOCUMENTATION PAGE

Form Approved
OMB No. 0704-0188

1. AGENCY USE ONLY (*Leave blank*)	2. REPORT DATE	3. REPORT TYPE AND DATES COVERED
	20 June 2002	Project Report

4. TITLE AND SUBTITLE

Analysis of SAR Image Formation Equations for Stationary and Moving Targets

5. FUNDING NUMBERS

C — F19628-00-C-0002

6. AUTHOR(S)

A.F. Yegulalp

7. PERFORMING ORGANIZATION NAME(S) AND ADDRESS(ES)

Lincoln Laboratory, MIT
244 Wood Street
Lexington, MA 02420-9108

8. PERFORMING ORGANIZATION REPORT NUMBER

FPR-14

9. SPONSORING/MONITORING AGENCY NAME(S) AND ADDRESS(ES)

DARPA, IXO
3701 N. Fairfax Drive
Arlington, VA 22203-1714

10. SPONSORING/MONITORING AGENCY REPORT NUMBER

ESC-TR-2001-074

11. SUPPLEMENTARY NOTES

None

12a. DISTRIBUTION/AVAILABILITY STATEMENT

Approved for public release; distribution is unlimited.

12b. DISTRIBUTION CODE

13. ABSTRACT (*Maximum 200 words*)

This report presents a detailed mathematical analysis of backprojection and "ω-k" (range migration) image formation equations for synthetic aperture radar (SAR). The image processor transfer function is computed for both stationary and moving targets, including antenna and target pattern effects. Assuming straight-line platform motion, it is demonstrated that both image formation algorithms provide exact focusing of stationary targets. Moving targets are displaced to false locations and blurred into elliptic or hyperbolic curves. Algorithms are suggested which will exactly refocus moving targets in SAR images based on only one unknown motion parameter. All results are derived without narrow-band, narrow-angle, or narrow-swath assumptions.

14. SUBJECT TERMS

15. NUMBER OF PAGES
50

16. PRICE CODE

17. SECURITY CLASSIFICATION OF REPORT	18. SECURITY CLASSIFICATION OF THIS PAGE	19. SECURITY CLASSIFICATION OF ABSTRACT	20. LIMITATION OF ABSTRACT
Unclassified	Same as Report	Same as Report	Same as Report